Materials and Structures (2009) 42:279–300
DOI 10.1617/s11527-008-9405-7

ORIGINAL ARTICLE

Coupling effect between masonry spandrels and piers

Paolo Foraboschi

Received: 30 October 2007 / Accepted: 1 July 2008 / Published online: 18 July 2008

Abstract In-plane performance of masonry load-bearing walls was tested in a quasi-static fashion by loading individual brickwork perforated walls with constant normal force and increasing lateral force. Fifteen full-scale unreinforced frames were constructed by professional bricklayers, from ordinary bricks and lime-mortar according to ancient techniques, so as to be representative of historic masonry. Each wall was subjected to two monotonic loadings (with unloading), up to the full drop-off in the stiffness and complete development of the kinematic mechanism. The specimens exhibited significant overstrength with respect to the strength provided by the masses and high deformation capacity, which are not adequately represented by code provisions for analysis of ancient masonry buildings. The overstrength is here described by several key parameters, namely: (1) Level of coupling piers by spandrels, (2) virtual work done by interlocking and friction forces, (3) and maximum tensile stress in the top spandrel and nodal panels. The paper attempts also to calibrate the behavior factors (q) for masonry frames that are not overly conservative, as code-prescribed q-factors are. Thus, another key issue in the paper is to derive q-factors directly on the basis of the measured values to reproduce the overstrength, allowing for the normal force in the piers and the masonry texture of the wall.

Keywords Behavior factors · Frame coupling · Masonry · Mechanisms · Monotonic unloading tests · Perforated wall · Mass strength · Overstrength · Textures · Unreinforced masonry

1 Introduction

This paper deals with the seismic behavior of brickwork and stonework vertical structures of historic buildings. More specifically, the object of this paper is in-plane seismic capacity of masonry load-bearing walls of existing constructions.

Many historical constructions are still in service, so to assess masonry buildings is a main concern of structural engineering. When the safety margins are no longer assured or prove inadequate for new structural demands, two are the options, namely: (1) To reduce the structural demand, or (2) to upgrade the structure. The first option is unacceptable for historical constructions since it tends to "fossilize" the building, whereas historical building conservation requires keeping the construction in service to satisfy present needs. If an existing construction that holds cultural value is unable to meet the present building, road, rail or waterway structural demands, thus, to upgrade the structure is the only satisfactory option.

P. Foraboschi (✉)
Dipartimento di Costruzione della Architettura,
Università IUAV di Venezia, ex Convento delle Terese,
Dorsoduro 2206, Venice 30123, Italy
e-mail: paofor@iuav.it

Strengthening historical buildings in order to prolong the service life poses serious concerns, since reinforcement techniques may guarantee an adequate increment in strength, stiffness and ductility, but usually do not fulfill aesthetic or restoration needs and sometimes do not guarantee durability. Hence, the crucial point is not to upgrade or retrofit the construction considering also conservation and restoration demands, but to assess safety as precisely as possible.

Historical buildings may not satisfy structural demand code since modern-day loads are far higher than the ones initially considered, or substantial alterations are made to meet present architectural requirements and demands. But above all, historical masonry buildings usually do not satisfy seismic demand code.

The response of historical structural systems to seismic excitation actually differs substantially from the response of more modern structural systems, but often is not as deficient as usually perceived and supposed by codes. The notable conservatism of the codes derives only in part from the poor performance and extensive damage shown at times by masonry structures in past earthquakes, but for the major part derives from the general conviction that it is more difficult to reach a precise analysis result for masonry structures than steel or concrete structures since, compared with steel or concrete materials, the properties of masonry material exhibit a greater degree of uncertainty due to the uncontrollability of handicraft.

The crucial point is that some of the favorable aspects of masonry seismic response are specific to the single structures so can hardly be generalized, while safety assessment methods established by current codes disregard the contributions to structural capacity that are neither standard nor usual. This means to allow only for the strength due to the masses, whose contribution is the only one that can be generalized for unreinforced masonry. This notable conservatism may be suitable for new masonry buildings, whose structure includes unreinforced masonry only marginally, since steel bars or beams reinforce the vast majority of masonry spandrels and piers, as well as floors and lintels are well connected to masonry walls. On the contrary, it may be not appropriate for the review of existing buildings, whose structure is entirely composed of unreinforced masonry, where unacceptable economic and cultural penalty could be imposed should seismic analyses allow only for the strength provided by masses. Highlighted are new seismic code provisions for ancient structures that have been adopted recently by a number of code bodies, in particular by 2003 Italian code (the last version is of 2005) [1], devoted to the design of structures for earthquake resistance, that are overly conservative.

Hence, ancient building conservation entails to point out the buildings whose current usage is definitely unable to meet present structural demand, and to avoid structural work stemming only from the great degree of uncertainty about actual capacity of masonry structures or from erroneous convictions about masonry response.

The excessive conservatism of codes is mainly due to the fact that code provisions do not consider the contribution of masonry tension strength and texture interlocking. Neglecting these contributions, the interaction between masonry spandrels and piers of perforated walls is totally disregarded. Thus, the coupling effect is a crucial point.

2 Position of the problem

Due to the small tensile strength and brittle behavior in tension of masonry material compared to the fairly high compressive strength (although the behavior in compression is brittle as well), together with the relatively large dimensions of the cross sections of vertical load-bearing structures, the controlling failure modes of masonry structures are rocking (Fig. 1) and sliding (Fig. 2) mechanisms. Conversely, crushing failure (included toe crushing) and diagonal tension are not the controlling failure modes, except for unusual configurations or special constructions [2–7]. As regards diagonal tension, while it is not an actual failure mode, conversely it may be the cause of diagonal cracks through joints and bricks. Thus, diagonal tension may initiate failure for shear mechanism, i.e., it may trigger a mode of failure whose cause is the shear action, as sliding mechanism (Fig. 2), but whose movement consists of translation of the masonry portion that results from diagonal cracks.

Accordingly, the load-carrying capacity of masonry structures is predicted by the kinematic mechanism analysis of rigid body movements,

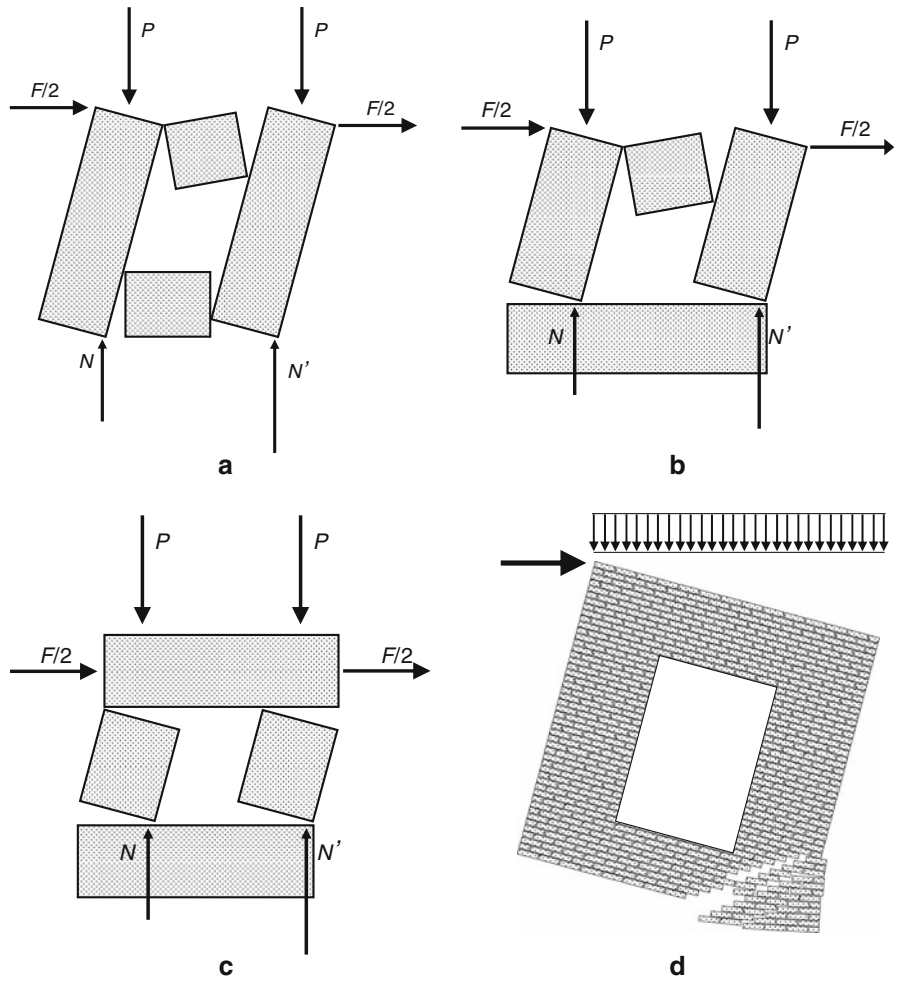

Fig. 1 Rocking failure modes of unreinforced masonry perforated wall: (**a**) lower, (**b**) intermediate, (**c**) upper, (**d**) and global overturning shapes of kinematic mechanism

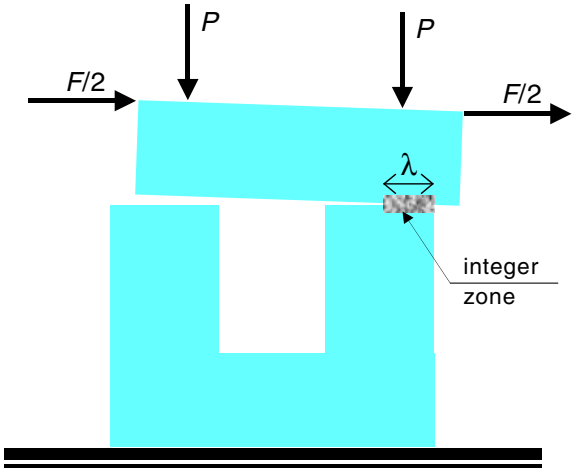

Fig. 2 Sliding failure mode of unreinforced masonry perforated wall

together with friction mechanism analysis (which includes the ultimate shear stress integrated over the uncracked part of the cross section, although this contribution is not substantial). On the contrary, no-tension analysis can only predict the stress distribution for given external loads but can not assess the safety condition, since safety of masonry structures depends neither on the maximum compressive stress, nor on the crushing strength. In masonry historical buildings, in fact, major dead loads were employed regardless the stress level, just to increase the masses that are lifted up by the rigid body movements of the kinematic mechanisms, so increasing the load-carrying capacity.

Some modern structural standards recognize that rocking and sliding (including shear failure) lie at the bottom of the resistance hierarchy of masonry

structures. This approach represents advancement with respect to the codes of past generation. If however the ultimate seismic capacity considers only the strength provided by the masses of the construction, code provisions result to be overly conservative, since in so doing assessment neglects any strength provided by masonry material (except for shear stresses, whose contribution however is marginal).

As regards the Italian seismic code [1], unreinforced masonry spandrels are assumed to be fully uncoupled with respect to supporting piers. As regards the Eurocode 8, the final version [8] specifies that (sec. 9.4.4) '*spandrels may be taken into account as coupling beams between two wall elements if they are regularly bonded to the adjoining walls and connected both to the floor tie beam and to the lintel below*'. Contrary to new spandrels, however, usually such connections do not exist in ancient spandrels. Thus, spandrels cannot be taken into account as coupling beams. Actually, ancient masonry structures do not fall within the scope of Eurocode 8.

Consequently, code provisions for horizontal resistance calculation of ancient masonry structures consist of the lower external lateral load that turns the structure into a kinematic mechanism, according to an analysis based on rocking and friction mechanisms. Hence, calculations of ultimate horizontal load disregard the contributions to load-carrying capacity that imply tensile stresses, in particular do not allow for any strength due to frame action of the perforated wall. In such codes, thus, only the behavior factors (q) could reproduce the strength that supplements the load-carrying capacity provided by masses. Conversely, the code-prescribed behavior factors are too low for this purpose, i.e., the q-factors take into account only hysteretic energy dissipation provided by masonry system, while the q-factors neglect coupling effect.

Unfortunately, the masses together with the code-prescribed behavior factors provide the masonry frame only with moderate theoretical capacity of withstanding lateral forces. As a result, the vast majority of historical buildings turn out to be seismically unsafe and thus require upgrading work. This requirement does not seem consistent with the numerous historical buildings that are still in service and exhibit marginal damage despite they have been struck by major earthquakes [9–12].

An historical building may really not satisfy seismic demand code despite its long service life. In fact, the return period of the design action for ultimate limit state is about half of millennium (and the return period for collapse limit state is more than two millenniums); so, even an historical building may have not yet met the expected seismic action. However, also a building survived a major earthquake without appreciable damage may be seismically inadequate. In fact, a building may have tolerated an intense earthquake only because its first natural frequencies are far from the peaks of the seismic action in the frequency domain, whereas it collapses if it is struck by an earthquake with the same intensity but adverse spectrum. Similarly, a building may have tolerated a major earthquake only because the horizontal action struck the building in its strong direction, while it fails if it is struck by an earthquake with the same intensity but in the weak direction. Moreover, the seismic capacity decreases throughout centuries, with the increasing of crack patterns.

On the other hand, the survival of great stocks of buildings proves that the mean seismic capacity of such buildings is considerably higher than code-prescribed seismic capacity, and masonry buildings may satisfy the demand code with minor upgrading work. This is the case of the historical buildings of Mediterranean basin that, as reported during major earthquakes, can perform quite well under certain circumstances, particularly if the out-of-plane overturning moment of the walls is resisted.

3 Scope of the paper

Several mathematical models, including "strong pier–weak spandrel", "equivalent frame" and "strong spandrel–weak pier", have been successfully employed to model perforated in-plane masonry walls [3–6, 9, 10, 13–17]. These models attempt to reproduce the effect of coupling piers by spandrels. However, model results are affected by the great degree of uncertainty of masonry properties. Therefore, the predictions of such models may be unreliable for assessing the load-bearing capacity and the safety performance of masonry structures. The relatively large discrepancies between model results necessarily entail the codes to ignore the

coupling between the spandrels and piers. Despite the code assumptions, yet, the models that incorporate a substantial coupling effect are the most consistent with experimental observation. Therefore, it would be worthwhile to develop knowledge in this field. This research aims at contributing to the topic of spandrels-piers coupling, in particular at defining how much spandrel may be taken into account as coupling beam.

4 Strength provided by masses

The strength provided by masses is dictated by rocking or sliding. As regards rocking, the strength derives from the masses that are lifted up and taken down by the rigid body movements of the kinematic mechanism (the former movements provide positive contributions while the latter negative contributions to strength). A rocking kinematic mechanism consists of a set of masonry portions joined by pins. A pin does not correspond to a hinge. Contrary to the common structural hinge, in fact (Fig. 1), the pin's position is on the boundary of the section (not on the centroid), only the relative opening of the two pinned sections is possible (the rotation is unilateral), and no plasticity and friction are displayed by a pin (the pin does not behave as plastic hinge).

The point is to determine the mechanism dictating the load-carrying capacity of the structure, whose shape mainly depends on the nodal panel (the intersection between pier and spandrel). Four are the possible shapes of rocking mechanism of perforated walls, namely: I—Lower; II—intermediate; III—upper; IV and global overturning (Fig. 1).

Lower, intermediate and upper shapes of mechanism (Fig. 1a–c) are the result of the piers in the condition of cantilever over the span extending from either the lower or the upper level of the bottom spandrel, to either the upper or the lower level of the top spandrel. By the in-plane deformation, thus, the piers rock about the leeward individual toe while the top spandrel rotates with respect to either the nodal panel, or the piers. The lateral strength of a mechanism derives from both the fraction of the total mass that is lifted up by the rigid body movements and from the lever arms of the masonry portions joined by pins, as shown by the virtual work equations (such equations are described in [18]). In the lower mechanism, the spandrel contributes to lateral strength only because of its mass, so the level of coupling piers by spandrels is the minimum. The opposite in the upper mechanism, where the spandrel contributes to lateral strength also because of its flexural and shear strength, so the level of coupling is the maximum. Consequently, the lateral external force in equilibrium with the lower mechanism is the minimum, and with the upper mechanism the maximum, among the three mechanism of Fig. 1a–c. Accordingly, the lower mechanism matches up with Italian code provision (strength by masses). The global overturning shape of mechanism (Fig. 1d) consists of the rigid rocking movement of the entire perforated wall. It occurs when the opening is small, otherwise the load-carrying capacity of the global overturning mechanism is greater than that of the upper one.

As regards sliding (Fig. 2), the shear resistance is given by the friction coefficient and the normal force, where the latter derives from the masses (strength by masses).

5 Description of experimental tests

The main objective of the tests described herein was to address the knowledge gap pointed out in Sects. 2 and 3, considering as well the numerous experimental results found in the technical literature. A range of experimental work has been carried out on the in-plane performance of masonry walls and panels, but they have often been limited to testing scale models, small panels, or these with artificially imposed boundary conditions. Conversely, a limited number of tests have been carried out on full-size specimens and relatively few experimental investigations have been conducted on complete structures. But above all, ancient masonry structures have been considered only occasionally. Although all the aforementioned studies provided valuable insight into nonlinear properties of masonry [2, 4, 7, 11, 16, 19–25], much work is still needed to characterize the true inelastic behavior of masonry walls.

5.1 Design of test structures

It was intended to represent the typical bearing wall structures of historical buildings. Window and door

openings, as well as historic mortar have a significant influence on the behavior and the ultimate capacity of these types of structure. The test structures were therefore single-story full-scale unreinforced brick masonry walls with opening, assembled by hydrated lime mortar (Figs. 3–12). Each specimen was hence composed of two piers, two spandrels and a lintel beam, with bed joints without cement.

All the walls were constructed by experienced masons, in line with the ancient rules of construction of the historical treatises, and a licensed masonry contractor experienced and skilled in restoration of old brickwork supervised. Insofar as possible, construction procedures were consistent with standard practice for historical buildings, and details were designed to promote the device of ancient masonry structures.

Several types of models were used to predict the response of the research perforated wall prior to test [26]. Theoretical results showed that the adopted geometry and arrangement allowed for the investigation of the main key parameters.

5.2 Description of specimens

Fifteen real brickwork frames were fabricated and then tested in a quasi-static fashion (Figs. 3–5). Brick nominal dimensions were 250 mm in length, 125 mm in width, and 61 mm in thickness. All the fifteen test frames had the same geometry and were composed of the same bricks and mortar. The dimensions of each frame were 3.06 m height × 3.12 m width, and of each opening 1.21 m height × 1.07 m width. Dimensions were chosen to represent common load-bearing perforated walls.

Fig. 3 Test perforated wall; texture 1

Fig. 4 Test perforated wall; texture 2 and test setup

The frames were composed of double wythe brick masonry; so, the wall thickness was 0.250 m (Fig. 5). This is the typical thickness of historic masonry bearing walls.

Five masonry textures were adopted; hence, three specimens per texture. The bond pattern was the same for all the frames, while the textures differed in the number of transverse bricks. From the first to fifth texture, an increasing number of bricks with the long side normal to the masonry surface were set. The adopted textures are representative of old Italian buildings and of those in other countries as well, since a texture is characterized by the number of transverse bricks per square meter.

The wall specimens were constructed and then exposed to strong rainwater as well as many sunny days for approximately 18 weeks before testing.

5.3 Material properties

Critical material properties typically used for design and safety assessment were measured using standardized tests, such as compression tests of square prisms of brick and masonry, as well as of cylinders of mortar, bond wrench, four-bricks direct shear tests, and tensile tests. Nominal dimensions of prism brick were 150 mm in length and 60 mm in side, and of cylinder mortar were 200 mm in length and 80 mm in diameter. The prisms of masonry were built of three bricks units put on top of each other, using the same mortar and the

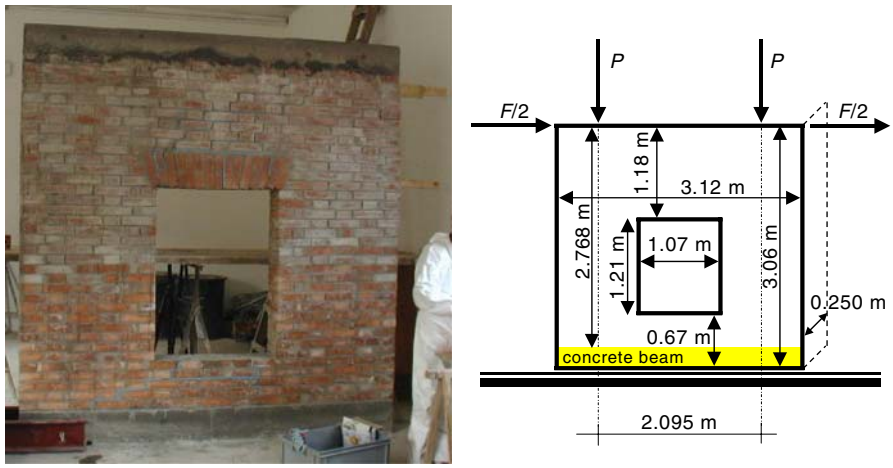

Fig. 5 Left: Elevation of the specimen. Right: Basic dimensions

Table 1 Key material properties measured (or experimentally deduced*) using standardized tests

Masonry (N/mm^2)		Bricks (N/mm^2)		Mortar (N/mm^2)	
Compressive strength, f_m	1.21	Compressive strength, f_b	2.36	Compressive strength, f_l	0.77
Modulus of elasticity, E_m	1,360	Modulus of elasticity, E_b	3,150	Modulus of elasticity, E_l	1,013
Tensile strength*, f_{mt}	0.08	Tensile strength, f_{bt}	0.14	Tensile strength, f_{lt}	0.05

same construction technique as was used for the test walls. Prisms and cylinders were subjected to the same environment conditions as the walls. The results of the material tests are given in Table 1.

5.4 Test rig

To simulate realistic boundary conditions, a 194 mm height concrete braced loading distribution beam was poured on the top of each wall and the brickwork was laid onto a 292 mm height concrete foundation beam fixed to the pavement of the laboratory (Fig. 7). The beams reproduced also the floors, including flexible floor diaphragms, since usually they are unreinforced. The net height of the brickwork was hence 2,574 mm.

In so doing, imposed displacements to the top of the leeward pier (pier at the side opposite to loading side) were essentially the same as those imposed to the top of the windward pier (pier at the loading side) and the shear action was well distributed in the piers. The concrete elements affected only slightly the coupling effect, since they were unreinforced and they cracked well before the initiation of coupling effect.

Relevant aspects of the design of the lintel pertain to the observed seismic response of historical buildings. Typically, masonry piers are not coupled by lintels over the window and door openings, due to the marginal anchorage and the brittle failure of historical lintels. To accomplish this, the opening was spanned by nonstructural lintel. The lintel was composed of quasi-vertical bricks, separated from the spandrel by 7 mm expansion joints to allow the spandrel to rotate relative to the piers without engaging the lintel, and not initiating the cracking and the failure of the lintel (Fig. 6).

Imitating typical method of constructing lintels in the past was the goal of this approach, as well as imitating typical ancient construction methods was the goal of the specimen design. First contact and damage of the lintel did not occur until the wall attained an overall drift level of 1.3%, at which point the expansion joint closed completely and the lintel engaged the adjacent spandrel (Figs. 6, 8 left). Thus, the use of nonstructural lintel prevented behaviors that are unrealistic in ancient buildings.

5.5 Testing procedure

To simulate the actual gravity loads on load-bearing walls that offset the lateral load, four vertical forces were applied at the top of each test wall. This was

Fig. 6 Closeup of the lintel beam during test 1–3, at an overall drift level of about 1.3%

Fig. 7 Test rig; concrete braced loading distribution beams

Fig. 8 Closeup of the lintel beam after test 1–3 (left) and 5–3 (right)

Fig. 9 Loading system: actuators and steel reaction frame

accomplished by four prestressing tendons (high tensile steel cables) and four actuators (Fig. 9), i.e., a vertical prestressing tendon and actuator per side of the masonry wall and per pier, to develop the required total level of clamping vertical load, P_v.

The main difficulty in using this approach was that as the pier's midheight horizontal displacement increased, the top of the wall height was raised slightly, thereby extending the actuators. However, the servocontrol that governed the actuators permitted to keep the clamping vertical force of each actuator nearly constant during each test (the prestressing force applied by each tendon varied less than $\pm 1\%$). Thus, the wall specimens did not suffer significant increases in precompression even at large displacements, and constant force assumption was considered to be largely acceptable during all the tests. Accordingly, each vertical tendon provided $P_v/4$. So, clamping vertical forces acted like real gravity loads.

Three levels of P_v were applied at each of the five textures: $P_v = 40$ kN (20 kN per pier), $P_v = 80$ kN (40 kN per pier) and $P_v = 140$ kN (70 kN per pier).

The tests were conducted in displacement control (Figs. 9–11), so as to capture also the softening branch of the load-deflection curve. The testing procedure included two loadings per wall with

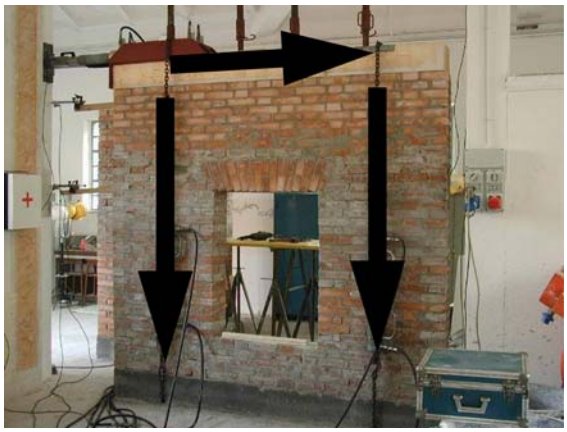

Fig. 10 Applied loads; the vertical top forces were kept constant during each test, while the horizontal lateral top force was increased up to reaching the maximum displacement

Fig. 11 Loading system: device to apply and smear the horizontal force

unloadings. The vertical force P_v was kept constant during each loading (and unloading), while the horizontal top force was monotonically increased (Fig. 10) up to reaching the maximum lateral displacement attainable (Fig. 13). The second loading was applied in the same direction, so the testing procedure consisted of a repeated loading with unloading and not a cyclic loading.

5.6 Experimental test setup and instrumentation

The test setup primarily consisted of five mounted servocontrolled hydraulic actuators (Figs. 4, 9), one providing an in-plane top horizontal force and four providing two in-plane vertical resultant forces, i.e., pier axial force. A steel reaction frame collected the reaction of the horizontal actuator. A strong floor, at

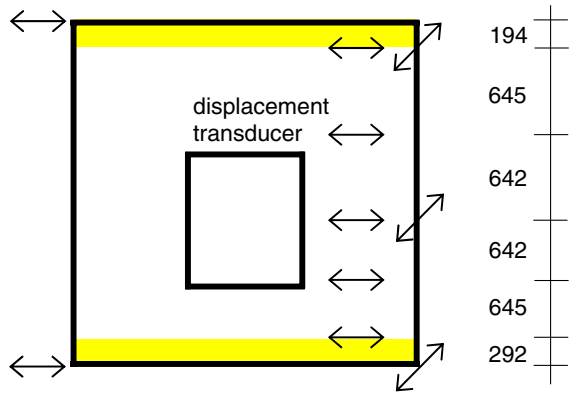

Fig. 12 Displacement transducers on the test specimen to record the displacements

which the concrete bottom beam was fixed by anchor bolts, collected the reactions of the vertical actuators. Lateral and verticals forces were measured by load cells positioned in series with the hydraulic actuators.

Displacement transducers were positioned to record the horizontal in-plane and out of plane displacements at several heights, to capture also the distribution of the strain acting on the wall (Fig. 12). Another 16 displacement devices were located throughout the wall to measure: Actuator displacements; horizontal slip of walls at construction joints; spandrel/lintel rotations over the opening. Moreover, potentiometers were used to measure the global vertical movements as well as to monitor sliding behavior, and strain gages with a 35 mm gage length to measure the strain.

6 Tests results: summary and detailed discussion

Each test is labeled by a two-digit number. The first digit indicates the level of the vertical load: $1 - P_v =$ 40 kN (i.e., 20 kN per pier); $2 - P_v = 80$ kN (i.e., 40 kN per pier); $3 - P_v = 140$ kN (i.e., 70 kN per pier). The second digit indicates the percentage of bricks set with the larger side across the wall thickness with respect to the wall surface: $1 = 2.5\%, 2 = 5.0\%$, $3 = 10.0\%, 4 = 15.0\%, 5 = 20.0\%$ (Figs. 13 and 14).

6.1 Load–displacement response

Coupling effect, to which the paper is devoted, is pointed out by the measurements of the top displacement transducers and the load cells, while the

Fig. 13 Some of the new response limit states exercised by the tests, attained by the perforated walls during the loadings (pull direction: first photograph). (**a**) Masonry textures number 5. The pier rocks about the leeward individual toe. Pier overturning produces first crack that here is shown at a drift of 1.45%. (**b**) Masonry texture 4. First crack during the first loading, when the windward pier tends to rock. (**c**) Cracking in the top spandrel during the second loading. Crack interlocking produces internal resisting couples. (**d**) Ultimate state of the top masonry spandrel at the end of the second loading

measurements of the whole mounted extensive instrumentation of Fig. 12 were here used only to check the load-deflection diagrams (while such results will be the subject of next papers).

The curves lateral force versus horizontal translation at the top of the wall are reported in the 15 diagrams of Fig. 14 (30 curves), in which the lower abscissa shows the displacement (in mm) applied at the top of the brickwork, while the upper abscissa shows the drift (in percentage), where the drift is defined as the lateral displacement (lower abscissa) divided by net wall height (i.e., 3.03 m). Moreover, the left ordinate shows the lateral force (in kN) associated with the displacement, while the right ordinate shows the ratio of the lateral force to the sum of the own weight of the mass portions involved in the mechanism (two piers and the upper spandrel = 23.38 kN) plus vertical top load P_v. In each diagram, the first loading is represented by the solid curve and the second loading by the dashed line.

6.2 Key experimental results

In Fig. 14, the circle represents the theoretical lateral top force that triggers the lower shape of mechanism (Fig. 1a), the square the intermediate (Fig. 1b), the rhombus the upper (Fig. 1c), the triangle the sliding mechanism (Fig. 2) calculated by using a friction coefficient of 0.4 and the test measured shear strength of 0.11 N/mm^2.

A summary of the key experimental results and a comparison of the test measurements with rigid body analytical predictions is given in Tables 2–4. The values of maximum experimental lateral load, F_{max}, and wall top-height displacement, d_{max}, when F_{max} was recorded, are respectively given in columns 2 and 6 for first loading, 8 and 12 for second loading. These tables list also the first and second loading drifts in columns 7 and 13 respectively. Moreover, the Tables 2–4 compare F_{max} to the strength obtained by the rigid body model for each of the three rocking mechanisms of Fig. 1a–c, and for each P_v. The ratio of F_{max} to the strength estimated, respectively, for lower mechanism, F_{Lw}, denoted λ, intermediate mechanism, F_{In}, denoted β, and upper mechanism, F_{Up}, denoted γ, are given (in that order) in columns 3, 4 and 5 for first loading, and in columns 9, 10 and 11 for second loading.

6.3 Interpretation of the load-deflection diagrams

To gain a better understanding of the findings of the research as presented in Fig. 14, this paragraph recalls the following results.

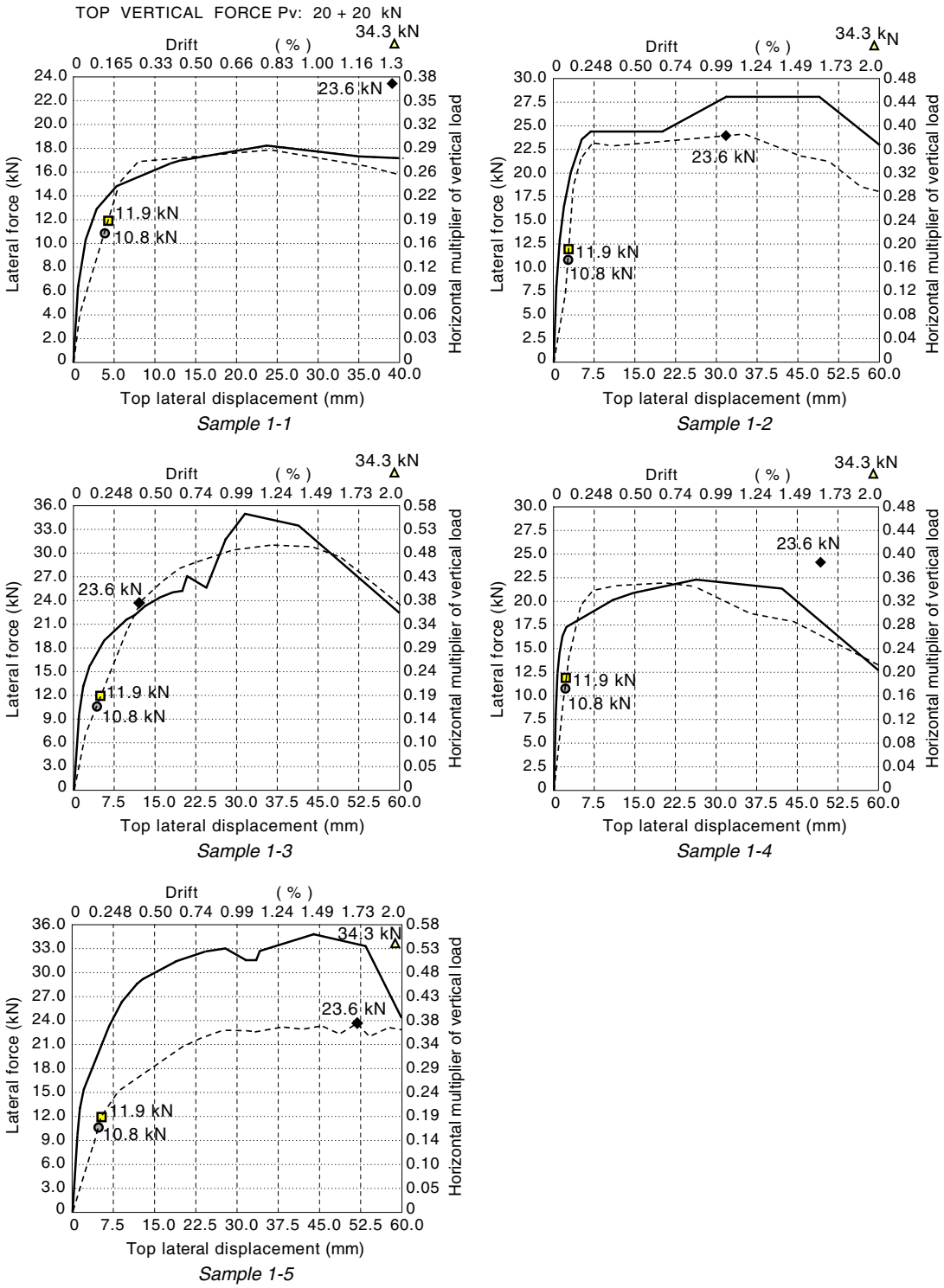

Fig. 14 Load–displacement response of the 15 perforated walls: solid line = first loading; dashed line = second loading. Rocking and sliding lateral forces calculated by the motion analysis of rigid bodies: lower mechanism (Fig. 1a) = shadowed circle; intermediate mechanism (Fig. 1b) = shadowed square; upper mechanism (Fig. 1c) = black rhombus; sliding mechanism (Fig. 2) = triangle

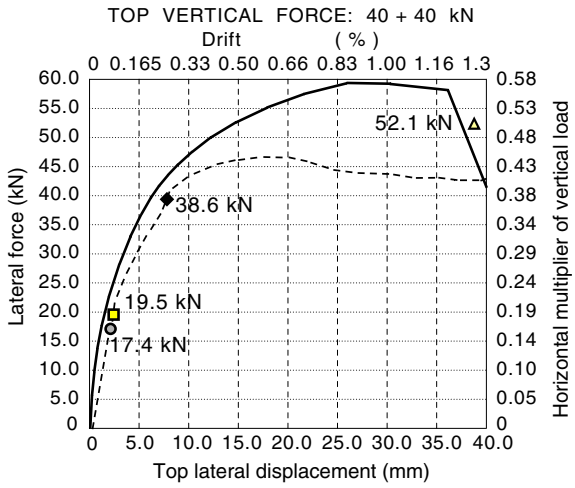

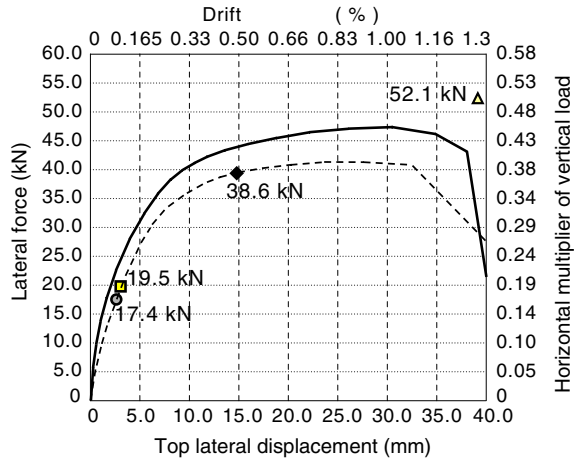

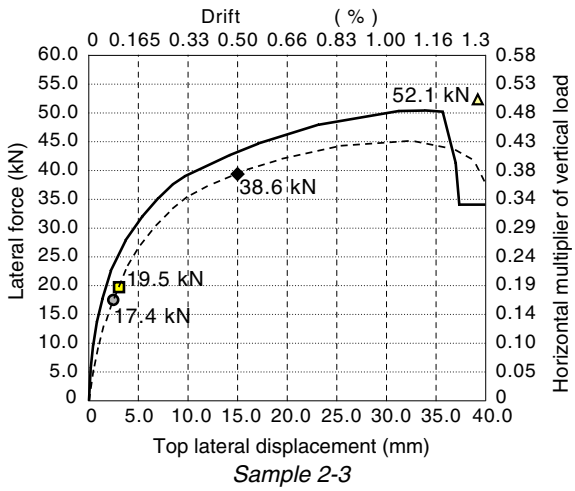

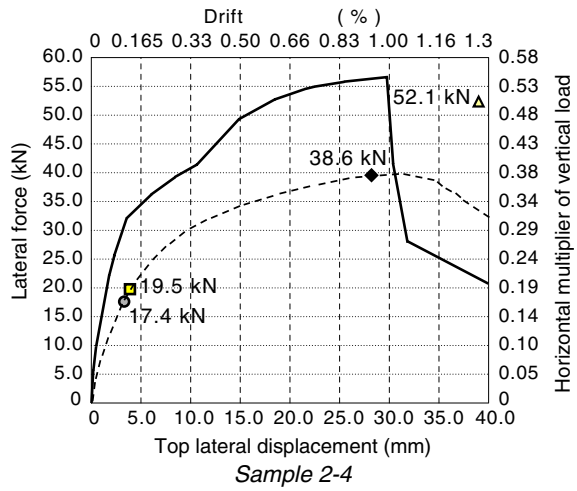

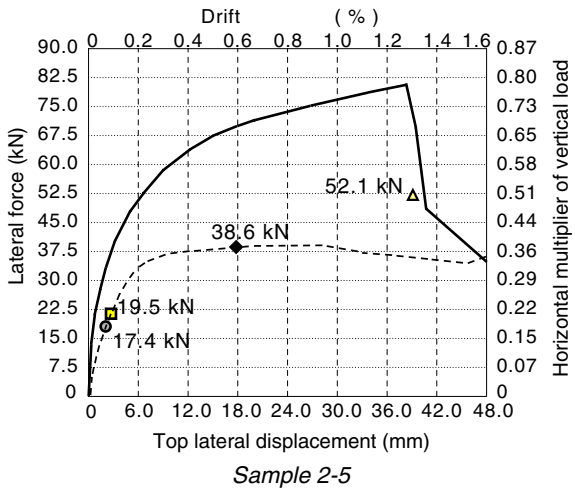

Fig. 14 continued

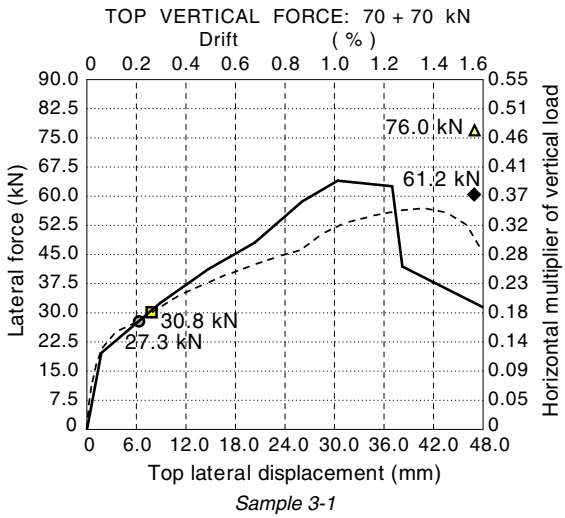

Sample 3-1

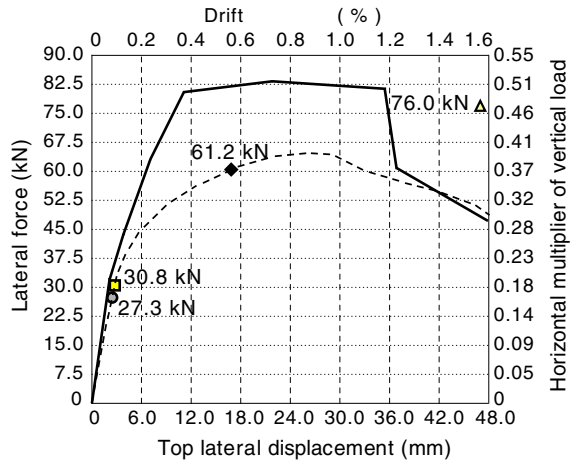

Sample 3-2

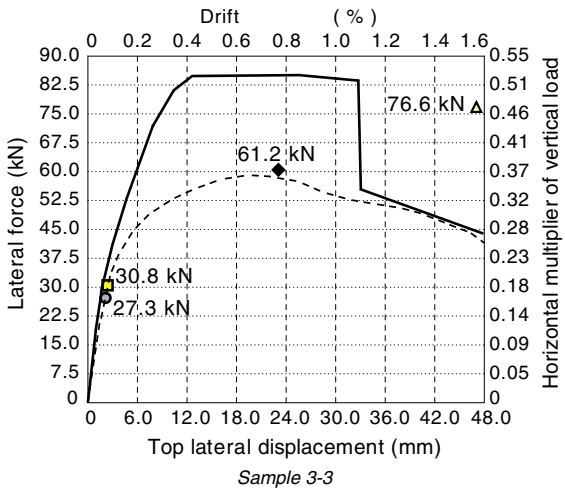

Sample 3-3

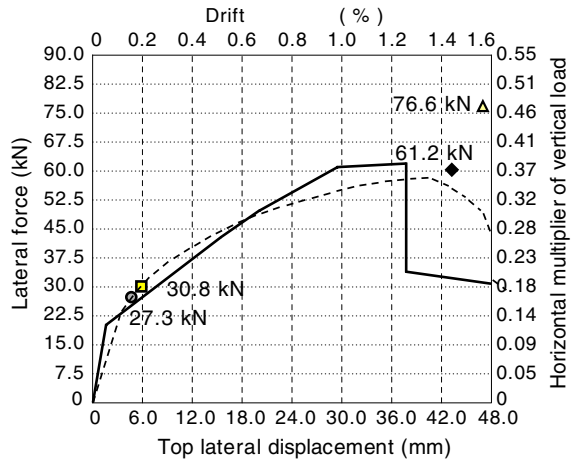

Sample 3-4

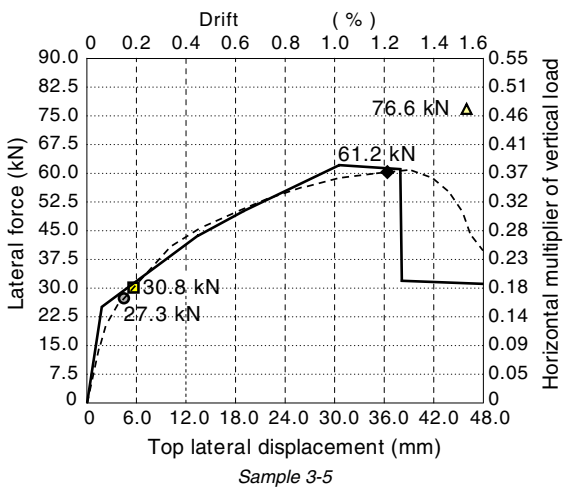

Sample 3-5

Fig. 14 continued

Table 2 Summary of test results for the set of five walls with vertical normal force $P_v = 20 + 20$ kN, where $\lambda = F_{max}/F_{Lw}$, $\beta = F_{max}/F_{In}$, $\gamma = F_{max}/F_{Up}$

	First loading						Second loading					
Wall Label	F_{max} kN	λ –	β –	γ –	d_{max} mm	δ %	F_{max} kN	λ –	β –	γ –	d_{max} mm	δ %
1–1	18.2	1.69	1.53	0.77	23.5	0.78	17.9	1.66	1.50	0.76	24.6	0.81
1–2	28.3	2.62	2.38	1.20	49.1	1.62	24.2	2.24	2.03	1.03	35.5	1.17
1–3	35.2	3.26	2.96	1.49	32.3	1.07	31.4	2.91	2.64	1.33	40.0	1.32
1–4	22.4	2.07	1.88	0.95	25.8	0.85	21.8	2.02	1.83	0.92	22.0	0.73
1–5	34.8	3.22	2.92	1.47	43.5	1.44	23.6	2.19	1.98	1.00	51.6	1.70

Table 3 Summary of test results for the set of five walls with $P_v = 40 + 40$ kN, where $\lambda = F_{max}/F_{Lw}$, $\beta = F_{max}/F_{In}$, $\gamma = F_{max}/F_{Up}$

	First loading						Second loading					
Wall Label	F_{max} kN	λ –	β –	γ –	d_{max} mm	δ %	F_{max} kN	λ –	β –	γ –	d_{max} mm	δ %
2–1	59.8	3.44	3.07	1.55	26.6	0.88	46.7	2.68	2.39	1.21	19.1	0.63
2–2	47.6	2.74	2.44	1.23	30.2	1.00	41.8	2.40	2.14	1.08	28.5	0.94
2–3	50.4	2.90	2.58	1.31	36.1	1.19	45.2	2.60	2.32	1.17	32.3	1.07
2–4	56.9	3.27	2.92	1.47	29.3	0.96	39.9	2.29	2.05	1.03	31.4	1.04
2–5	80.9	4.65	4.15	2.10	38.6	1.27	38.8	2.23	1.99	1.01	27.0	0.89

Table 4 Summary of test results for the set of five walls with $P_v = 70 + 70$ kN, where $\lambda = F_{max}/F_{Lw}$, $\beta = F_{max}/F_{In}$, $\gamma = F_{max}/F_{Up}$

	First loading						Second loading					
Wall Label	F_{max} kN	λ –	β –	γ –	d_{max} mm	δ %	F_{max} kN	λ –	β –	γ –	d_{max} mm	δ %
3–1	64.2	2.35	2.08	1.05	31.1	1.03	57.5	2.11	1.87	0.93	39.2	1.29
3–2	83.1	3.04	2.70	1.36	21.8	0.72	65.1	2.38	2.11	1.06	28.1	0.93
3–3	84.6	3.10	2.75	1.38	26.7	0.88	59.4	2.18	1.93	0.97	20.5	0.68
3–4	62.9	2.30	2.04	1.02	38.3	1.26	58.4	2.14	1.90	0.95	40.2	1.33
3–5	62.4	2.29	2.03	1.02	31.8	1.05	61.3	2.25	1.99	1.00	39.5	1.30

- First cracking always occurred at a load significantly lower than the peak of the curve.
- All the curves exhibit high deformation capacity, even for the second loadings, while do not exhibit any quickly drop off in the horizontal resistance, i.e., softening behavior is not pronounced.
- The higher the normal force, the greater is the slope of the pre-peak branch. The greatest slope was for the intermediate number of transverse bricks (texture 3).
- For low normal force and few transverse bricks, second loading post-peak branch tends to overlap first loading one, whilst it is very different for high normal force and many transverse bricks. The strength of the second loading beyond the peak is sometimes above the strength of the first loading. This observation can be explained by an increment of interlocking and friction forces at the second loading, due to more closed fracture surfaces and to the plasticity-induced crack-closure.

6.4 Interpretation of the behavior throughout the loading and limit states

Visual inspections of the specimens revealed some interesting effects and trends.

- First cracking occurred at the construction joint between the piers and the bottom spandrel for textures 1–4, and at a lower level for texture 5 (Fig. 13a–b). First cracking initiated in the horizontal mortar joints at the windward pier side and developed into a horizontal crack. Bottom cracks occurred well before top cracks.
- Observed mode of failure was the intermediate shape for textures 1–4 and the lower shape for texture 5. Conversely, F_{max} resulted almost always greater even than the lateral force that triggers the upper mechanism F_{Up} (Figs. 13, 14; γ of Tables 2–4).
- The lateral strength calculated for the friction mechanism (triangle) is almost always greater than for the upper mechanisms (rhombus). Before piers or spandrels may slide, hence, piers rocked about their individual leeward toes, while the top spandrel rocked as well, so sliding mechanism was not observed. Thus, friction failure mode can be ignored in the discussion of the results.
- Crushing strength had no significant effect on the response of the test structures.
- First considerable damage was a diagonal crack that appeared in the leeward top nodal panel. Crack initialized at the center of the nodal panel and propagated diagonally until it reached the upper and lower corners of the nodal panel. After a slight increase of drift, a similar crack developed in the windward top nodal panel (Fig. 15).
- Nodal panels cracking occurred at the first loading, when the drift was substantially lower than the ultimate drift. Increasing the drift, especially at the second loading, cracking propagation formed edge-notched cracks in the top spandrel (Fig. 13c–d).
- In all the walls, hence, first damage occurred in the nodal zones and consisted of a dense array of cracks, which were interlocked rather than stress free. The observation that cracks were interlocked and that first damage occurred in the nodal zone is contradictory to many conventional models in which cracks are modeled as pins and the nodal zones are modeled as rigid zones. Since such models influence the seismic codes, this observation may explain the large discrepancy existing between the code provisions and the good performance or at least moderate damage shown often by masonry structures in past earthquakes (as developed in the chapter 6.5).

6.5 Interpretation of nodal panels cracking and correlation with coupling effect

Cracks in the nodal panels initialized at the center of the nodal panel, due to the high tensile stress concentration at 45° provoked by the shear action (Fig. 15a), and propagated diagonally up to diagonal tension failure (Fig. 15b). Conversely, cracks in the nodal panels were not the result of any frame action, since each crack did not initiate at the edge of the

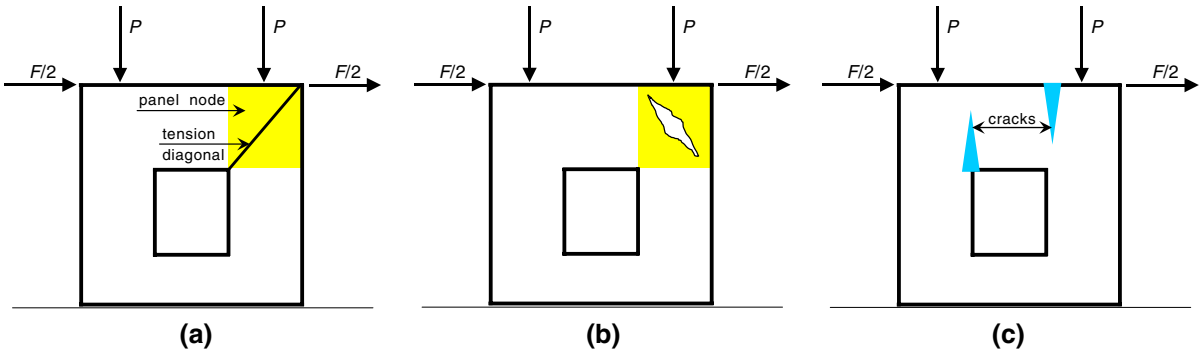

Fig. 15 Observed cracking in the top spandrel. (**a**) Tensile stresses in the nodal panel; (**b**) explanation of the cracking. (**c**) Cracking that would occur if the perforated wall behaved as a frame

nodal panel, i.e., frame behavior was not observed (Fig. 15c).

The nodal panel that failed was the leeward one, rather than the windward one, because the leeward pier transmitted a fraction of total shear action greater than the windward pier. This was a consequence of a compressive normal force greater in the former than in the latter, due to the overturning resisting moment provided by the piers through the lever arm resulting from the span between the piers.

Since the dense array of diagonal cracks behaved as interlocked, the interfaces of each crack were partially prevented from rotating one with respect to the other. This explains why the mechanical interlocking occurring at the crack interface during in-plane deformation reinforced the participation of the top spandrel. Observed substantial spandrel participation can be described by a couple transmitted across the cracks due to interlock effects. Hence, crack state impacted the response of masonry perforated walls, since cracks supplied additional strength and deformation capacity to resist the lateral load by means of interlock engaged by the dense array of edge-notched cracks (*cohesive cracks*) developed even at major drifts and at the second loading, which affected substantially the lateral behavior of the perforated wall.

The lateral force remained close to the maximum as long as the couples transmitted across cohesive cracks were held by interlocking. Since cracks did not release interlocking even for high drifts, the development of the mechanism was resisted by the interconnections engaged between crack edges and the lateral force remained relatively close to the maximum for a wide range of drift, even at the second loading. This result has a great relevance for the seismic evaluation of unreinforced masonry buildings, although the degradation due to cyclic loading implies a reduction of such benefit.

7 Overstrength with respect to the lower mechanism

Analyses of the observed behaviors were mainly devoted to the horizontal resistance that supplements the strength of the lower mechanism, hereafter referred to as *overstrength*. The overstrength derives from coupling effect between spandrels and piers. Since first cracking totally disconnected the bottom spandrel from the piers, coupling effect is provided only by the top spandrel. Consequently, coupling effect ensues from the couple developed by the internal shear force acting in the two cross-sections at the ends of top masonry spandrel. In fact, such shear forces result in a global overturning resisting moment, C, developed by the piers normal forces N acting over the lever arm $L = 1.025 + 1.07 = 2.095$ m between the axes of the two piers (Fig. 5, right), where N is the total normal force acting in each pier minus the normal force due to the vertical loads (i.e., minus the fraction of normal force due to the own weights plus P_v).

The maximum value of the global external moment, M_e, is given by F_{max} over the lever arm given by the height of the brickwork, that is $H = 2.768$ m. Due to coupling effect, $M_e = F_{max} \cdot 2.768$ kN m is resisted partially by the lower mechanism and partially by C. Thus, the overstrength corresponds to C. The writer believes that the most logical representation of the overstrength is the following parameter θ (Table 5) that compares the overstrength with the total strength (the latter is equal to the maximum applied global overturning external moment).

$$\theta = \frac{C}{M_e} = \frac{L \cdot N}{H \cdot F_{\max}} = \frac{1.025 \cdot N}{2.768 \cdot F_{\max}} = 0.37 \cdot \frac{N}{F_{\max}} \tag{1}$$

An additional representation of the coupling effect can be gained by the ratio ζ of F_{max} to the lateral top force F_g that triggers the global overturning mechanism (Fig. 1d).

$$\zeta = \frac{F_{\max}}{F_g} \tag{2}$$

Consider that the own weight of the brickwork plus upper beam is 33.94 kN, the overturning lever arm is 3.06 m, and the resisting lever arm under the assumption that the wall rocks about its individual leeward toe is 3.12 m (i.e., not considering that the pin takes place inside the section, as conversely shown in Fig. 1d), the following values were obtained for the overturning force F_g: for $P_v = 40$ kN, $F_g = 40.48$ kN; for $P_v = 80$ kN, $F_g = 60.88$ kN; for $P_v = 140$ kN, $F_g = 91.46$ kN, by which ζ was calculated (Table 5).

The overstrength can also be expressed by the field of tensile stresses in the top spandrel at the ultimate. However, this representation is not objective since

Table 5 Ratio θ of Eq. 1 and ratio ζ of Eq. 2

	1: $P_v = 40$ kN				2: $P_v = 80$ kN				3: $P_v = 140$ kN			
	First loading		Second loading		First loading		Second loading		First loading		Second loading	
	θ	ζ	θ	ζ	θ	ζ	θ	ζ	θ	ζ	θ	ζ
1	0.41	0.44	0.40	0.42	0.71	0.93	0.63	0.73	0.57	0.65	0.53	0.59
2	0.62	0.68	0.55	0.58	0.63	0.74	0.58	0.65	0.67	0.85	0.58	0.66
3	0.69	0.84	0.66	0.75	0.65	0.78	0.62	0.70	0.68	0.86	0.54	0.60
4	0.52	0.54	0.50	0.52	0.69	0.89	0.56	0.62	0.57	0.64	0.53	0.60
5	0.69	0.84	0.54	0.57	0.78	1.26	0.55	0.60	0.56	0.64	0.55	0.63

First row = Total clamping vertical force; first column = Masonry texture type

Table 6 Maximum tensile stress for each test

	1: $P_v = 40$ kN				2: $P_v = 80$ kN				3: $P_v = 140$ kN			
	First loading		Second loading		First loading		Second loading		First loading		Second loading	
1	0.687	0.202	0.676	0.193	2.259	1.293	1.764	0.873	2.425	1.072	2.172	0.857
2	1.069	0.526	0.914	0.395	1.798	0.902	1.579	0.716	3.139	1.678	2.459	1.101
3	1.330	0.748	1.186	0.626	1.904	0.992	1.707	0.825	3.195	1.727	2.244	0.918
4	0.846	0.337	0.823	0.318	2.149	1.200	1.507	0.655	2.376	1.030	2.206	0.886
5	1.314	0.735	0.583	0.376	3.056	1.971	1.466	0.619	2.357	1.014	2.315	0.979

First row = Total clamping vertical force; first column = Masonry texture type. Left column of each loading: Elastic model of the framed structure. Right column of each loading: Stress field that balances F_{max} with the minimum peak of tensile stress (lower bound theorem for masonry structures)

stresses have to be theoretically deduced from an assumed masonry constitutive law while can not be experimentally measured. A variety of elastic and inelastic approaches were used to investigate the response of the masonry structures tested in the laboratory, and the most logical models to represent the stress field resulted to be (Table 6): (1) A finite element elastic model of the framed structure; and (2) the stress field that balances F_{max} with the minimum peak of tensile stress, in accordance with the lower bound theorem for masonry structures. The real maximum tensile stress is comprised between these two types of results.

8 Pier height model of overstrength

Consider that the theoretical value of F_{max} depends on the shape of the mechanism, that the measured value of F_{max} is greater than the value of F_{max} associated with the observed kinematic mechanism, and that the shape is identified by the effective pier height involved in mechanism, this is tantamount to assuming an effective pier height taken as lesser than the actual one. Hence, the equivalent pier height approach disregards the actual governing mechanism but describes the horizontal resistance by adequately tuning the height of the piers. Taking pier height as the height of adjacent opening plus the two spandrels, as in the codes of ancient buildings, results in overly conservative strength estimation, whereas taking pier height as the height of the adjacent opening, the horizontal resistance of the test structures results in a sufficiently accurate and conservative strength approximation.

Although this approach is expedited, it is not completely effective since it control neither the masonry texture nor the normal force. Consequently, the estimation provided by this approach may be precise for these frames, but this precision is due to compensating errors. It is concluded that these competing factors neutralized one another and results in a seemingly accurate estimation of strength. This type of accidental accuracy of equivalent pier height

Table 7 Virtual work done by the interlocking and friction forces at the ultimate

	1: $P_v = 40$ kN				2: $P_v = 80$ kN				3: $P_v = 140$ kN			
	First loading		Second loading		First loading		Second loading		First loading		Second loading	
1	8.19	35	7.80	34	52.39	67	35.36	58	43.42	52	34.71	46
2	21.32	58	15.99	51	36.53	59	28.99	53	67.99	63	44.59	53
3	30.29	66	25.35	62	40.17	61	33.41	57	69.94	64	37.18	48
4	13.65	47	12.87	45	48.62	66	26.52	51	41.73	51	35.88	47
5	29.77	66	15.21	50	79.82	76	25.09	50	41.08	51	39.65	50

First row = Total clamping vertical force; first column = Masonry texture type

For each loading: left column = Work done for a unitary angle of rotation and for each hinge (kN m/rad); right column = Percentage of work done by the interlocking and friction forces with respect to the total work done by the system forces at the ultimate (%)

approach should not be relied upon when dealing with configurations different from the ones by which pier height was tuned.

9 Interlocking and friction model of overstrength

The most effective approach to allow for overstrength of masonry frames is to model its actual source. Overstrength derives from the opposition to kinematic rigid relative movements given by interlocking from indentation of cracks interfaces and friction from compressive internal forces, which result in a couple transmitted across each crack that supplements the lower mechanism strength.

To describe the actual source of overstrength, the virtual work equation that governs the equilibrium of the rigid bodies has to include also the virtual work done by the interlocking and friction forces in resisting relative rotation of the two pinned sections. The test results permitted the estimation of such work and to express it an applicable form (Table 7). In fact, the work done by the interlocking and friction forces is equal to the work done by the external horizontal force F_{max}, minus the sum of the works done by the weight of the masonry portions lifted up and taken down by the rigid body movements of the mechanism and by the vertical precompression forces.

10 Recommendations

Codes devoted to masonry buildings allow for coupling effect between masonry spandrels and piers only if the tensile force of the internal couple is furnished by steel bars or beams. Unfortunately, this condition pertains only to new masonry but usually is not satisfied by ancient masonry. Since tensile forces are not provided and tensile stresses are neglected, consequently coupling effect is disregarded for unreinforced masonry. Therefore, the code-prescribed horizontal resistance of ancient masonry perforated wall is the lateral load that triggers the lower shape of mechanism.

Accordingly, almost all the seismic codes of last generation devoted to ancient buildings (e.g. Italian code [1]) assess the ultimate seismic capacity of masonry building as the minimum lateral load applied to the building that turns the weakest load-bearing wall into the lower kinematic mechanism, and assess the ultimate seismic demand as the lateral load generated by the elastic spectrum (i.e., design spectrum) lowered by the behavior factor q. Since maximum horizontal load calculation disregards coupling effect between masonry spandrels and piers, only the code-prescribed behavior factors may allow for such effect.

The behavior factors of masonry buildings are given by the following expression

$$q = \alpha \cdot \xi \cdot q' = \alpha \cdot q_0 \tag{3}$$

in which $q_0 = \xi \cdot q'$ allows for ability of dissipating kinetic energy ensured by unreinforced masonry structures and α for overstrength provided by the capacity curve obtained by non-linear static analysis of the building. For instance, [1] adopts $q' = 2.0$ and $\xi = 0.75$ if the stiffness center is eccentric with respect to the mass centroid and therefore the energy dissipation is concentrated in few walls, otherwise $\xi = 1$ (i.e., $q_0 = 1.5 \div 2$). As regards α, this coefficient is given by the expression

$$\alpha = \frac{\alpha_u}{\alpha_1} \tag{4}$$

in which α_u corresponds to the ordinate of the peak and α_1 to the ordinate of the point where first masonry wall reaches its maximum strength capacity. Overstrength α should be related to the strength that is considered in the seismic assessment. Thus, the maximum strength capacity of first masonry wall should coincide with the lower mechanism, since coupling effect is neglected so lateral strength derives only by the masses. Accordingly, α_u is the horizontal resistance of the building (maximum lateral load), and α_1 should coincide with the lateral load applied to the building that triggers the lower mechanism of the weakest wall. Hence, α should quantify the overstrength due to both the actual strength of the wall with respect to the strength of the lower mechanism and to the multiple walls, stories, and spans with respect to the individual wall.

Italian seismic code [1] places the upper limit of $\alpha = 1.8$ for multi-story buildings (and $\alpha_u = 90\%$ of the α-peak). Since $\lambda \gg 1.8$ (Tables 2–4), contrary to the above α disregards individual wall overstrength but considers only multiple walls, stories, and spans. Therefore, α does not reproduce exhaustively the overstrength (i.e., code-prescribed α does not reproduce the above-mentioned definition), since it neglects coupling effect. So, code-prescribed q-factors are overly conservative.

Let α_{Lw} be the value of α that corresponds to the activation of the lower mechanism of the weakest wall. Since α_{Lw} corresponds to the code-prescribed maximum lateral load that the building can bear, the behavior factor should refer to a coefficient α whose denominator is α_{Lw}, whilst α_1 is the actual ultimate lateral load of the weakest load-bearing wall. Hence, the following coefficient α' has to replace α of Eq. 4:

$$\alpha' = \frac{\alpha_u}{\alpha_{Lw}} \geq \alpha \tag{5}$$

Let us define μ as the ratio of lateral force applied to the whole building that causes the collapse of the first masonry wall to the lateral force applied to the whole building that turns such wall into the lower shape of mechanism, i.e.,

$$\mu = \frac{\alpha_1}{\alpha_{Lw}} \tag{6}$$

Recall the ratios λ (Tables 2–4); both μ and λ represent the overstrength of the wall, but μ as a component of the bearing structural system, while λ as individual structure.

The difference $\mu - \lambda$ depends on the amount of nonlinearity that the structural system displays for α_1. The main source of nonlinearity is cracking, whose initiation and propagation is marginal for $\alpha \leq \alpha_1$ (in fact, $\alpha = \alpha_1$ is approximately the limit of linearity of the capacity curve). The following assumption is therefore admissible:

$$\mu = \lambda \quad \text{i.e.,} \quad \frac{\alpha_1}{\alpha_{Lw}} = \frac{F_{\max}}{F_{Lw}} \tag{7}$$

Rearranging Eq. 5 gives the following form of coefficient α':

$$\alpha' = \frac{\alpha_u}{\alpha_1} \cdot \frac{\alpha_1}{\alpha_{Lw}} \tag{8}$$

Replacing the right term of Eq. 7 into Eq. 8 gives

$$\alpha' = \frac{\alpha_u}{\alpha_1} \cdot \frac{F_{\max}}{F_{Lw}} \tag{9}$$

Equation 9 leads to

$$\alpha' = \frac{\alpha_u}{\alpha_1} \cdot \lambda \equiv \alpha \cdot \lambda \tag{10}$$

The following expression is hence obtained for the q-factors of masonry buildings

$$q = q_0 \cdot \alpha \cdot \lambda \tag{11}$$

in which α allows for overstrength of the whole building, while λ for overstrength of individual wall. Hence, λ takes into account the actual horizontal resistance of the wall with respect to that of the lower mechanism (coupling effect). Equation 11 differs in form from code-prescribed q-factors for the presence of λ (where $\lambda > 1$).

This research has tuned λ so as to provide design values (Table 8), taking into account the masonry texture and the level of compressive force in the piers, on which overstrength significantly depends, as proved by test results.

Since code expressions ought to include safety factors that account for several aspects, the following Eq. 12 has to replace Eq. 11:

$$q = \frac{q_0 \cdot \alpha \cdot \lambda}{\Psi_1 \cdot \Psi_2} \tag{12}$$

in which Ψ_1 accounts for the variability in the measured values used for the calibration of λ, and Ψ_2 for degradation due to cyclic loading. Since all

Table 8 Design values of coefficient λ of Eqs. 11 and 12 as a function of the average compressive normal stress, σ_a, in the piers (first row), and the masonry texture (first column) as well as the percentage of transverse bricks (second column)

	%	$\sigma_a \leq 0.20$ N/mm^2	$0.20 < \sigma_a < 0.40$ N/mm^2	0.40 N/mm^2 $\leq \sigma_a$
1	2.5	1.25	1.50	1.60
2	5.0	1.35	1.60	1.65
3	10.0	1.45	1.75	1.70
4	15.0	1.55	2.00	1.75
5	20.0	1.60	2.10	1.80

specimens were different, hence no covariance can be derived from the experimentation. Since the tests were monotonic with unloading, hence they can not capture degradation due to cyclic loading, which is very important in general, and particularly important if friction-related mechanisms are involved [25]. Thus, further experimentation is necessary to calibrate Ψ_1 and Ψ_2. For the time being, the author feels compelled to place the lower limit of $\Psi_1 \cdot \Psi_2 = 1.5$. The proposed overall safety factor $\Psi_1 \cdot \Psi_2 = 1.5$ seems to be a low one, in fact it is the material safety factor used in the Eurocodes for concrete; safety factors for masonry (which is characterised by higher covariance than concrete) start from 1.5 and, depending on the type of masonry units etc., can reach up to 3.0. Moreover, only Ψ_1 is a real safety factor, while Ψ_2 is a mechanical parameter, since it accounts for the cyclic nature of earthquake loading. However, 1.5 is a low value only for high values of q, while for moderate and low values of q it seems to be appropriate. Accordingly, the writer believes that the limit $q < 5$ should be respected for historical masonry buildings, or alternatively the value $\Psi_1 \cdot \Psi_2 = 3.0$ should be used for $q > 5$.

11 Conclusion

Although out-of-plane wall response is the principal vulnerability of many unreinforced masonry buildings, in-plane wall response may frequently be vulnerability as well. But while the former is really a major problem, the latter problem is often the result of the notable conservatism of current codes whereas real vulnerability is frequently not excessive. Moreover, to improve out-of-plane wall response needs minor strengthening work, while to improve in-plane response needs major work.

Motivated by the demonstrated excessive conservatism of the codes on upgrading design of ancient masonry structures for earthquake resistance, a comprehensive research program was developed by the author [18, 26–30], which included several experimental studies on component-level response and culminated with the present monotonic in-plane tests of masonry perforated walls. More specifically, here a range of experimental work has been carried out on in-plane performance of fifteen perforated walls composed of two piers and two spandrels, assembled by a lime mortar and constructed imitating typical ancient construction methods and rules.

Although the cyclic loading is a more severe and accurate load condition [12, 25] than the adopted quasi-statical monotonic loading (particularly when friction-related mechanisms are involved, as in the perforated wall), nevertheless the tests replicate seismic loading as well, since second loading with unloading can in part capture degradation due to seismic response. Moreover, to interpret the results of cyclic loadings is more difficult than of monotonic loadings, in order to achieve general formulations. Last but not least, monotonic loading reproduces push-over static analysis.

Since structural behavior of ancient masonry buildings derives from the behavior of individual frames, hence results of the test program assist to explain the response of an entire masonry building subjected to an earthquake.

The experimental results suggest that the flexural strength and shear strength of the spandrel play an important role in nonlinear lateral load resistance and in seismic capacity of masonry perforated walls. Moreover, this full-scale seismic simulation tests under laboratory conditions show that even lime-mortar brickwork can exhibit large deformations under extreme seismic loads by inelastic flexural

behavior in predetermined locations. These findings that are in accordance with the available literature on masonry, clearly highlight the importance of such characteristics in the response of masonry walls and the need of calibrating code provisions as regards coupling between unreinforced masonry spandrels and piers. This should be done by appropriate nonlinear structural models. However, nonlinear analysis may be excessively complicated in practical applications. Thus, coupling effect should be taken into account by changing the behavior factor rather than by nonlinear modeling.

Thus, one of the key objectives of the paper is the calibration of code provisions for analysis of masonry buildings, in particular to derive behavior factors (q) that are not overly conservative, as the code values are. First, some parameters are defined to describe overstrength; then, an attempt is made to derive q-factors directly on the basis of the measured values. To this objective, lateral strength that was found to supplement strength by mass has been incorporated in the behavior factors by a coefficient λ that increases the q-factors, which allows for masonry texture of the wall and normal force in the piers. Differently form current code provisions, the proposed values of λ recognize the demonstrated seismic low in-plane vulnerability of many masonry load-bearing walls. As a result, even the actual state, or however minor strengthening work, may effectively switch the critical component to in-plane seismic action, from inadequate to adequate for earthquake resistance.

On other result is that the quickly cut down of the stiffness always occurs for a drift greater than 1.0% (and often than 1.5%) and that the ultimate drift is greater than 2%. These results can be advantageously used in push-over analyses.

In order to have more confidence on the coupling effect, however, cyclic-static tests and maybe dynamic tests are needed, further than monotonic loadings.

References

1. OPCM 3274/2003 (OPCM 3431/2005) Design of structures for earthquake resistance. (In Italian: Primi elementi in materia di criteri generali per la classificazione sismica del territorio nazionale e di normative tecniche per le costruzioni in zona sismica). Italy, G.U. 08.05.2003, 293 pp
2. Seible F, Priestley MJN, Kingsley GR, Kürkchübasche AG (1994) Seismic response of full-scale five-story reinforced-masonry building. J Struct Eng 120(3):925–946. doi: 10.1061/(ASCE)0733-9445(1994)120:3(925)
3. Venu Madhava Rao K, Venkatarama Reddy BV, Jagadish KS (1996) Flexural bond strength of masonry using various blocks and mortars. Mater Struct 29(2):119–124. doi: 10.1007/BF02486202
4. Magenes G, Calvi MG (1997) In-plane seismic response of brick masonry walls. Earthq Eng Struct Dyn 26(11):1091–1112. doi:10.1002/(SICI)1096-9845(199711)26:11<1091::AID-EQE693>3.0.CO;2-6
5. Kappos AJ, Penelis GG, Drakopoulos CG (2002) Evaluation of simplified models for lateral loads analysis of unreinforced masonry buildings. J Struct Eng 128(7):890–897. doi:10.1061/(ASCE)0733-9445(2002)128:7(890)
6. Valluzzi MR, da Porto F, Modena C (2004) Behavior and modeling of strengthened three-leaf stone masonry walls. Mater Struct 37(3):184–192. ISSN: 1359–5997
7. Griffith MC, Lam NTK, Wilson JL, Doherty K (2004) Experimental investigation of unreinforced brick masonry walls in flexure. J Struct Eng 130(3):423–432. doi: 10.1061/(ASCE)0733-9445(2004)130:3(423)
8. EN1998-1 (2004) Design of structures for earthquake resistance. General rules, seismic actions and rules for buildings. Eurocode 8. ISBN 058045872-5; Committee reference: B/525/8, 232 pp
9. Tena-Colunga A (1992) Seismic evaluation of unreinforced masonry structures with flexible diaphragms. Earthq Spectra 8(2):305–318. doi:10.1193/1.1585683
10. Bruneau M (1994) State-of-art report on the seismic performance of unreinforced masonry buildings. J Struct Eng 120(1):230–251. doi:10.1061/(ASCE)0733-9445(1994)120:1(230)
11. Sucuoğlu H, Erberik A (1997) Performance evaluation of a three-storey unreinforced masonry building during the 1992 Erzincan earthquake. Earthq Eng Struct Dyn 26(3):319–336. doi:10.1002/(SICI)1096-9845(199703)26:3<319::AID-EQE645>3.0.CO;2-C
12. Bommer JJ, Magenes G, Hancock J, Penazzo P (2004) The influence of strong-motion duration on the seismic response of masonry structures. Bull Earthq Eng 2(1):1–26. doi:10.1023/B:BEEE.0000038948.95616.bf
13. Gambarotta L, Lagomarsino S (1997) Damage models for the seismic response of brick masonry shear walls. Part i: the mortar joint model and its applications. Earthq Eng Struct Dyn 26(4):423–439. doi:10.1002/(SICI)1096-9845(199704)26:4<423::AID-EQE650>3.0.CO;2-#
14. Lee JS, Pande GN, Kralj B (1998) A comparative study on the approximate analysis of masonry structures. Mater Struct 31(7):473–479. ISSN: 1359–5997
15. Mistler M, Butenweg C, Meskouris K (2006) Modelling methods of historic masonry buildings under seismic excitation. J Seismol 10(4):497–510. doi:10.1007/s10950-006-9033-z
16. Tianyi Y, Moon FL, Leon RT, Kahn LF (2006) Analyses of a two-story unreinforced masonry building. J Struct Eng 132(5):653–662. doi:10.1061/(ASCE)0733-9445(2006)132:5(653)
17. Massart TJ, Peerlings RHJ, Geers MGD (2007) An enhanced multi-scale approach for masonry wall computations with localization of damage. Int J Numer Methods Eng 69(5):1022–1059. doi:10.1002/nme.1799

18. Foraboschi P (2001) Strength assessment of masonry arch retrofitted using composite reinforcements. Mason Int J Br Mason Soc 15(1):17–25, Surrey, UK Summer 2001
19. Calvi MG, Kingsley GR, Magenes G (1996) Testing of masonry structures for seismic assessment. Earthq Spectra 12(1):145–162. doi:10.1193/1.1585872
20. Tomaževič M, Klemenc I (1997) Verification of seismic resistance of confined masonry buildings. Earthq Eng Struct Dyn 26(10):1073–1088. doi:10.1002/(SICI)1096-9845(199710)26:10<1073::AID-EQE695>3.0.CO;2-Z
21. Griffith MC, Vaculik J, Lam NTK, Wilson J, Lumantarna E (2000) Cyclic testing of unreinforced masonry walls in two-way bending. Earthq Eng Struct Dyn 29(12):1797–1813. doi:10.1002/1096-9845(200012)29:12<1797::AID-EQE987>3.0.CO;2-D
22. Recommendations of RILEM TC 127-MS (2001) Tests for masonry materials and structures. 34(3)
23. Zonta D, Zanardo G, Modena C (2001) Experimental evaluation of the ductility of a reduced-scale reinforced masonry building. Mater Struct 34(10):636–644. ISSN: 1359–5997
24. Ewing BD, Kowalsky MJ (2004) Compressive behavior of unconfined and confined clay brick masonry. J Struct Eng 130(4):650–661. doi:10.1061/(ASCE)0733-9445(2004)130:4(650)
25. Oliveira DV, Lourenço PB, Roca P (2006) Cyclic behaviour of stone and brick masonry under uniaxial compressive loading. Mater Struct 39(2):247–257. ISSN: 1359–5997
26. Foraboschi P (2007) UnReinforced and FRP—reinforced masonry perforated walls: experimental and theoretical analyses. Text in English. Materiali ed Approcci Innovativi per il Progetto in Zona Sismica. ReLUIS, International Scientific Publisher, Milan, pp 239–246
27. Foraboschi P (2000) Experimental and theoretical analysis of masonry vaults with FRP reinforcements. In: Proceedings advanced composite materials in bridges and structures. 3rd International conference on ACMBS III MCAPC, Ottawa, Canada, 15 August 2000, pp 629–636
28. Foraboschi P (2001) On the seismic analysis of masonry arch bridges. In: Proceedings: ARCH'01. Third international arch bridges conference, Paris, France. Presses de l'école nationale des Ponts et chaussées, Parigi, Francia, pp 607–613
29. Foraboschi P (2002) Art of building and mechanical behavior of masonry panels. In: Proceedings of the British Masonry Society: sixth international masonry conference, London, UK, vol 9, pp 132–139
30. Foraboschi P (2004) Strengthening of masonry arches with fiber-reinforced-polymer strips. J Compos Constr 8(3):1–12. doi:10.1061/(ASCE)1090-0268(2004)8:3(191)